Polymer Motion at the Crossover from Rouse to Reptation Dynamics

D. Richter,* L. Willner, and A. Zirkel

Institut für Festkörperforschung, Forschungszentrum Jülich, 52425 Jülich, Germany

B. Farago

Institut Laue-Langevin, 38042 Grenoble, France, and Laboratoire Léon Brillouin (Laboratoire Commume, CEA/CNRS), Saclay, France

L. J. Fetters and J. S. Huang

Exxon Research and Engineering Corporation, Annandale, New Jersey 08801

Received April 4, 1994; Revised Manuscript Received August 10, 1994®

ABSTRACT: Employing neutron spin-echo spectroscopy, we have studied the dynamic structure factors for the relaxation of a single chain in polymer melts. We have varied the molecular weights through the transition region from unrestricted Rouse dynamics to entanglement controlled behavior. Investigating the dependence of the dynamic structure factor on the momentum transfer Q, it is possible to access the different relaxation modes separately. We found that, depending on their spatial extension in relation to the entanglement distance, larger scale relaxations are successively slowed down compared to Rouse relaxation. A comparison with macroscopic diffusion and viscosity data yields excellent internal consistency. Furthermore, we solve explicitly the generalized Rouse model by Hess[12] and compare its predictions to our data. Fitting only two parameters, all the Q and molecular weight dependent structure factors can be well reproduced.

1. Introduction

In the so-called plateau regime of the dynamic modulus long-chain polymer melts respond elastically like rubbers to external strain. In analogy to rubber elasticity, which originates from the entropy elasticity of polymer strands between permanent cross-links, the interpretation of the viscoelastic properties of polymer melts is based on the existence of a temporary network brought into existence by the entanglements of mutually interpenetrating long-chain molecules.[1] The distance between entanglements d introduces an intermediate dynamic length scale which for long chains is much shorter than the chain dimension but larger than the typical length of the monomeric building blocks. In the reptation theory this length becomes the step length of the course-grained chain profile and the diameter of the coaxially surrounding tube modeling the topological constraints. In this model chain motion is restricted to the tube which can only be left at its ends.[2–5] Though the entanglement distance is of crucial importance for our picture of polymer viscoelasticity, this length has only recently been identified directly on a microscopic scale[6,7] by neutron spin-echo (NSE) spectroscopy.

In order for entanglement constraints to become effective, the polymer chains have to exceed a critical molecular weight, M_c, corresponding roughly to 2.5 times the size of the entanglement strand in the entangled melt.[1] In this regime the melt viscosity η changes from $\eta \sim M$ (M = molecular weight of the chains) to $\eta \sim M^{3.4}$ and the self-diffusion coefficient is expected to cross over from the bead friction controlled Rouse behavior $D \sim 1/M$ to reptation-dominated diffusion $D \sim 1/M^2$. In the crossover regime the concept of well-defined stable constraints is not operational and chain relaxation may happen by both reptation-like diffusion along the chain profile and lateral motion as a consequence of constraint-release processes. Pearson has experimentally addressed the crossover phenomena on polyethylene melts.[8,9] He found a diffusion coefficient $D \propto 1/M^2$ through the whole transition regime. Such behavior has been traced to the drastic change of the monomeric friction coefficient as a consequence of the strong increase of free volume caused by reducing the chain length. If one takes out the free volume effects by investigating the molecular weight dependence of $D\eta/\varrho$, a sharp transition at $M_c = 5000$ ($T = 175$ °C) is observed. Considering the entanglement molecular weight $M_e = 2000$ as observed with NSE, the value for $M_e \simeq 2.5\, M_e$ is in the usual range.[10]

The mathematical description of chain relaxation in the melt uses normal modes, the geometrical structure of which relates to the random-coil conformation of the chains.[2] Without topological constraints these modes become the well-known Rouse modes[11] whose relaxation is determined by the entropy elasticity of the chains. Topological constraints will change the relaxation spectrum for each mode differently but not their spatial extension; the chain remains Gaussian.[12]

In this work we report on an investigation of the dynamic structure factor from single protonated polyethylene (PE) chains in deuterated PE melts by varying the molecular weight through the critical range and using neutron spin echo spectroscopy.[13] The different spatial ranges of the various modes lead to a distinct dependence on the momentum transfer $Q = 4\pi/\lambda \sin\theta$ (λ = neutron wave length, 2θ = scattering angle) for each mode. Exploiting this Q dependence, it has become possible for the first time to analyze separately the relaxation behavior of the different large-scale relaxation modes in polymer melts. Other than in the case of light scattering, where great difficulties were encountered in separating out the influence of the first Zimm modes on the relaxation spectrum in dilute polymer solutions,[14] neutron scattering allows an easy observation on the natural length scale of the relaxation modes,

® Abstract published in *Advance ACS Abstracts,* November 1, 1994.

0024-9297/94/2227-7437$04.50/0

Table 1. Molecular Weights and Heterogeneity Indices of Polybutadiene Precursor Polymers[a]

precursor polymer	$M_w \times 10^{-3}$	M_w/M_n	sample
PBd-6	2.0	1.07	PE-2
h PBd-6	2.05	1.07	
PBd-4	3.6	1.04	PE-3.6
h PBd-4	3.4	1.04	
PBd-11	4.8	1.03	PE-4.8
h-PBd-11	4.5	1.03	
PBd-3	6.5	1.02	PE-6.5
h PBd-3	6.6	1.02	
PBd-10	13.0	1.02	PE-13
h PBd-10	13.0	1.02	
PBd-8	36.0	1.02	PE-36
h PBd-8	34.0	1.02	
PBd-2	73.2	1.02	PE-70
h-PBd-2	70.5	1.04	

[a] The PEB-2 samples were obtained by hydrogenation or deuteration, respectively.

leading to large effects in the dynamic structure factor. With increasing molecular weight we find a successive slowing down of the first modes. The relaxation times are stretched particularly if the spatial extent of a mode exceeds a distance corresponding the entanglement mesh in the long-chain melt. Diffusion coefficients and viscosities evaluated from the dynamic structure factors agree well with macroscopic results on the same polymer. In a further step we present a solution of the generalized Rouse model put forward by Hess,[12] who derived an explicit expression for entanglement friction on the basis of excluded-volume forces. We compare our data with the predictions of this model and find overall excellent agreement with the predicted dynamic structure factors using only two adjustable parameters in order to describe all momentum transfer and molecular weight dependent spectra.

2. Experiment and Results

The polyethylene samples were prepared via saturation of polybutadiene precursor polymers. The polybutadienes were prepared via standard anionic polymerization techniques: *tert*-butyllithium, purified by sublimation, was the initiator. Size-exclusion chromatography was used to evaluate the heterogeneity indices. The saturation by hydrogen or deuterium of the polydienes was done by using palladium on barium sulfate. The procedure followed that of Gehlsen and Bates.[15] NMR analysis showed that saturation levels above 99.9% were obtained. The saturation procedure yielded a poly(ethylene-1−butene) copolymer, which is designated as PEB−2, where the integer denotes the approximate number of ethyl branches per 100 backbone atoms. It essentially resembles polyethylene. All samples are blends of a deuterated matrix and protonated chains. In each case the protonated fraction amounted to 12%. Table 1 lists the prepared samples and gives their molecular characteristics.

The neutron scattering experiments were carried out at the MESS neutron spin-echo spectrometer at the Orphée-Reactor in Saclay. In an NSE experiment the neutron polarization P is measured as a function of the applied guide field H for various scattering angles. For a coherently scattering specimen $P(Q,H)$ directly gives the normalized scattering function $S(Q,t)/S(Q,0)$, where t is the time which is proportional to the guide field H.[16] The scattering contrast arises from the difference in scattering length of the deuterated polymer matrix and the protonated chains. Under these conditions the coherent scattering of the individual chain or the intrachain pair correlation function is measured. In order to relate to earlier experiments on high molecular weight PEB-2 chains,[6,7] the experiment was performed at 509 K. Degradation of the polymers was avoided in storing the samples in sealed niobium containers under nitrogen. The background arising from the deuterated matrix (nearly entirely inelastic scattering) and

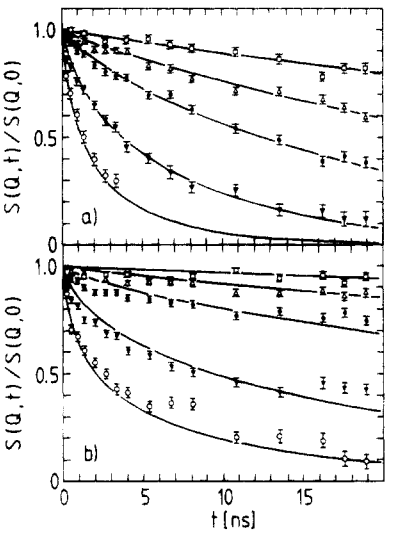

Figure 1. Dynamic structure factors for PEB-2 polymer melts of different molecular weights: (a) $M_W = 2.0 \times 10^3$; (b) $M_W = 4.8 \times 10^3$. The Q values are from top to bottom $Q = 0.037$, 0.055, 0.077, 0.115, and 0.155 Å^{-1}. The solid lines in a and b display the results of the mode analysis (see text).

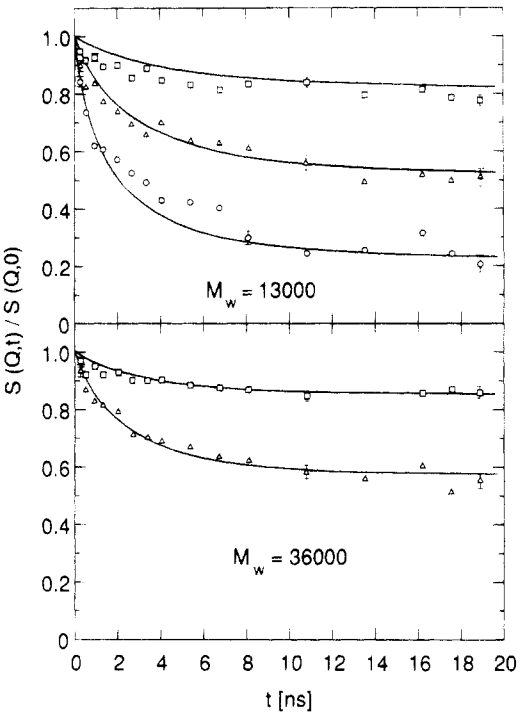

Figure 2. Dynamic structure factors for PEB-2 polymer melts of higher molecular weights. For the upper spectra the Q values are from top to bottom $Q = 0.077$, 0.115, and 0.155 Å^{-1}. The lower two spectra were taken at $Q = 0.077$ and 0.115 Å^{-1}. The solid lines represent a fit with the Ronca model (see text).

from the container were measured separately and subtracted with the appropriate transmission factors. Resolution corrections were performed using the instrumental resolution function obtained from a strongly scattering vycor glass standard.

Figure 1 presents as examples experimental spectra obtained for samples with molecular weights of 2×10^3 and 4.8×10^3 covering the transition region. Figure 2 displays data from longer chains with molecular weights of 13×10^3 and 36×10^3. Comparing the spectra from the short and long chains, their qualitative differences are obvious. While the dynamic structure factors from the short chains decay strongly, the spectra from the long-chain melts after an initial rapid decay exhibit long time plateaus signifying the tube constraints. We note, however, that increasing the molecular weight through the reptation transition reduces the spectral decay considerably. For example, at $Q = 0.115$ Å^{-1} the spectrum from the

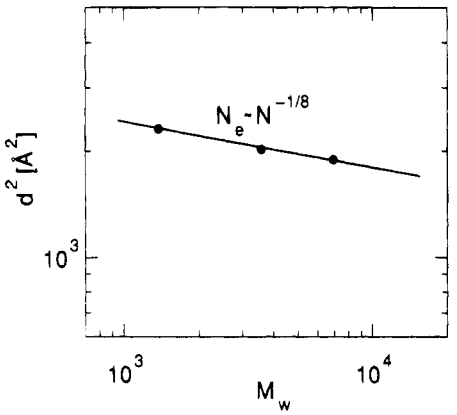

Figure 3. Entanglement distance d^2 as a function of molecular weight as obtained from the Ronca analysis (see also Table 2).

Table 2. Entanglement Distances d for the PEB-2 Samples of Higher Molecular Weights As Found by an Analysis in Terms of the Ronca[17] Model

		d (Å)	
sample	T (K)	Ronca	rheology (long chains)
PE13	509	47.8 ± 1	35 (373) PE
PE36	509	45.4 ± 0.6	42 (509 K) PEB-7
PE70	509	43.5 ± 0.7	

$M_W = 2 \times 10^3$ sample decays to about 0.1, while that from the $M_W = 4.8 \times 10^3$ chains only falls off to about 0.4. Thus it appears that in this molecular weight regime considerable constraints on chain relaxation are exerted. Inspection also reveals that at higher molecular weights, between 1.3×10^4 and 3.6×10^4, the long time spectral decay is still decreasing, indicating a persisting increase of constraints even at molecular weights much much higher than M_c.

A simple model allowing a numerical calculation of the dynamic structure factor $S(Q,t)/S(Q,0)$ for the motion of long chains under the influence of entanglement constraints has been proposed by Ronca[17] on the basis of a generalized Rouse model. In the Langevin equation for segmental motion this model treats the influence of topological constraints in terms of a memory function containing a time-dependent entanglement friction function. The resulting dynamic structure factor has been found to provide a reasonable description of the experimental spectra from long-chain polymer melts; though in detail deviations are present. Here we use the model, in order to parametrize the spectra obtained from the longer chains and in particular to extract the entanglement distances or tube diameters for the different molecular weights. The solid lines in Figure 2 display the results of a fit with the Ronca model. Table 2 presents the resulting entanglement distances (we include an earlier result on a $M_W = 7 \times 10^4$ chain[7]). Figure 3 displays the molecular weight dependence of d graphically. The observed trend is compatible with a weak power law dependence of the entanglement molecular weight M_e on M ($M_e \sim M^{-1/8}$).

3. Mode Analysis

Now we focus on the lower molecular weight samples. In order to analyze these spectra quantitatively, we cannot resort to asymptotic scattering functions like those for the Ronca model[17] or the Rouse model[18] which are only valid for very long chains. For short chains we have to consider the relaxation in terms of distinct chain modes. The trajectory of a Gaussian chain can be decomposed into Fourier components x_p

$$x_p = \frac{1}{N}\sum_n r_n(t) \cos\left(\frac{pn\pi}{N}\right) \tag{1}$$

where r_n are the vectors determining the positions of the chain segments and N is their number. We would like to emphasize that for a *Gaussian* chain the Fourier decomposition of eq 1 leads to normal modes independently; how complex the involved relaxation processes may be.[12] Concerning their spatial structure, these modes are the well-known Rouse modes. In terms of these Rouse modes the dynamic structure factor of the relaxing Gaussian chain has the general form:[2]

$$S(Q,t) = \frac{1}{N}\exp\left(-\frac{Q^2}{6}\langle[x_0(t) - x_0(0)]^2\rangle\right) \times \left\{\sum_{m,n}\exp\left[-\frac{1}{6}Q^2l^2\left|m-n\right| - \frac{4R_g{}^2Q^2}{\pi^2}\sum_{p=1}^{N}\frac{1}{p^2} \times \cos\left(\frac{p\pi m}{N}\right)\cos\left(\frac{p\pi n}{N}\right)(1 - \langle x_p(t)\, x_p(0)\rangle)\right]\right\} \tag{2}$$

Thereby, x_0 describes the center of mass coordinates, R_g the radius of gyration, N the number of chain segments, and l the segment length ($l^m = C_\infty l_0{}^2 = 13.76$ Å^2; l_0 = bond length, C_∞ = characteristic ratio[19]). The relaxation dynamics are buried in the detailed time dependence of the correlators $\langle x_p(t)\, x_p(0)\rangle$ describing the temporal development of a mode "p". In the case of Rouse motion, where the surrounding chains provide only the heat bath and relaxation occurs under the influence of entropic restoring forces and segmental friction, the normalized correlators read

$$\langle x_p(t)\, x_p(0)\rangle = \mathrm{e}^{-\nu_p{}^0 t}$$

$$\nu_p{}^0 = \frac{p^2}{\tau_R};\quad \tau_R = \frac{\zeta N^2 l^2}{3\pi^2 kT} = \frac{N^2}{W\pi^2} \tag{3}$$

$$\frac{1}{6}\langle[x_0(t) - x_0(0)]^2\rangle = D_R t = \frac{kT}{N\zeta}t$$

where ζ is the monomeric friction coefficient, D_R the Rouse diffusion coefficient, and W the Rouse rate. For more generalized relaxation behavior the correlators will assume a different time dependence. In the next paragraph we shall use the *ansatz* of Hess[12] to calculate explicitly the time dependence for a system with entanglement friction.

How can one hope to sort out the contributions of different modes or Fourier components to the relaxation behavior of $S(Q,t)$? Here the ability of neutron scattering to observe molecular motions directly on its natural time (t) and length (Q) scales facilitates a separation of the contribution of different modes to $S(Q,t)$: Different modes impact $S(Q,t)$ in different Q ranges. Since $S(Q,t)$ does not simply decompose into a sum or product of contributions from the different modes, this Q dependence is not easily visualized. In order to arrive at some transparency, we take the following approach. We consider the maximum relaxation a given mode p may exert on $S(Q,t)$. This maximum contribution is reached if $\langle x_p(t)\, x_p(0)\rangle = 0$ for this mode (eq 2). In order to make the picture simple, we freeze all other modes: $\langle x_s(t)\, x_s(0)\rangle = 1$ for $s \neq p$. This cancels all other mode contributions in eq 2. With this in mind we define mode contribution factors

$$R_p(Q) = \sum_{m,n} \exp\left\{ -\frac{1}{6}Q^2 l^2 |m-n| - \frac{4R_g{}^2 Q^2}{\pi^2}\frac{1}{p^2}\cos\left(\frac{p\pi m}{N}\right)\cos\left(\frac{p\pi n}{N}\right)\right\} / S(Q,t=0) \quad (4)$$

They describe to what extent a mode p may relax $S(Q,t)$ in the limit of long times ($t \rightarrow \infty$) and under the premise that all other modes are not active. Or in other words $R_p(Q) = S(Q,t\rightarrow\infty)_p/S(Q,t=0)$ displays to which asymptotic value $S(q,t)/S(Q,0)$ may decay under the action of a given mode p. Note, because of the $\Sigma_{m,n}$ in eq 2, $S(Q,t)$ is not simply given by a product of the different $R_p(Q)$—interference effects are important. Nevertheless, the $R_p(Q)$ display well in what Q range different modes become active.

Figure 4 presents mode contribution factors for the two low M_W polymers considered in Figure 1. The vertical lines indicate the experimental Q values. Viewing the contribution factors for the PE-2 sample, we realize that at the two smallest experimental Q values basically only translational diffusion plays a role (it appears as a front factor in eq 2). At $Q = 0.077$ Å^{-1} the first relaxation mode comes into play. For $Q = 0.115$ Å^{-1} we get a significant contribution from the second mode. Finally, at $Q = 0.155$ Å^{-1} higher modes contribute. As may be seen from the lower part of Figure 4 with increasing molecular weight, the onset of mode contributions is shifted toward lower Q. This Q-dependent onset of the different normal modes in the dynamic structure factor facilitates a separate determination of the relaxation dynamics of these modes.

In a first step we fitted the spectra in terms of the unrestricted Rouse modes using eqs 2 and 3. With the exception of the lowest molecular weight, where a reasonable fit may be obtained, this approach fails, yielding strongly molecular weight dependent Rouse rates and wrong spectral shapes. In order to improve this approach, while keeping the number of parameters limited, in a first iteration we kept the exponential decay of the normal modes but allowed for relaxation rates to depend beyond the p^2 Rouse prediction on the mode number. For this purpose we define relaxation rates

$$\tilde{\nu}_p = \frac{\pi^2 p^2}{N^2} W_p \quad (5)$$

where the basic rate W depends on the mode number. Explicitly, the fitting included independent relaxation rates for the first three modes, another rate for all higher modes, and the translational diffusion coefficient. The solid lines in Figure 1 display the resulting theoretical spectra. Table 3 presents the result for $W_p(M)$.

In order to demonstrate the contribution of the different normal modes to the relaxation of $S(Q,t)$, in Figure 5 for the PE-3.6 sample we compare calculated dynamic structure factors successively including an increasing number of modes with the experimental spectra. Thereby, we used the final result of a joint fit of all spectra to eq 2 as a basis. Figure 5a displays the contribution of translational diffusion. Only for the lowest momentum transfer $Q = 0.037$ Å^{-1} does translational diffusion describe the spectral decay. Figure 5b presents $S(Q,t)$ after the inclusion of the first mode: Now the long time behavior is well depicted, while for

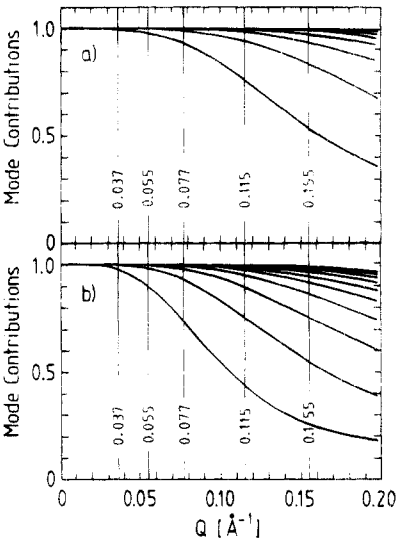

Figure 4. Contribution factors $R_p(Q)$ of the different modes to $S(Q,t)/S(Q,0)$ (see text) for the (a) $M_W = 2.0 \times 10^3$ and (b) $M_W = 4.8 \times 10^3$ samples. The experimental Q values are indicated by vertical lines. The Q-dependent decay of $R_p(Q)$ decreases with increasing mode number. Thus, the strongest decay relates to the first mode and so on.

short times the chain relaxes much faster than calculated, indicating the effect of higher modes. Parts c–e of Figure 5 demonstrate how the agreement between the experimental spectra and the result of the mode analysis improves in including more and more modes. Figure 5e presents the final results which show excellent agreement between theory and data.

This example was meant to demonstrate that a mode analysis of the spin-echo data may be performed sensitively. We realize that step by step different $Q - t$ regions in $S(Q,t)$ are affected. This allows a separation of the different modes.

Figure 6 presents the obtained relaxation times $\tau_p = 1/\tilde{\nu}_p$ for the first four modes as a function of molecular weight. The lines in the lower part of the figure display the Rouse prediction $\tau_p \sim N^2/p^2$; the lines in the upper part depict the experimental N dependence for the low modes and serve as a guide to the eye. For the higher modes and the lower molecular weights or equivalently for times shorter than about 5 ns the normal modes decay according to unrestricted Rouse relaxation—the $p - N$ dependence of the relaxation times are in accordance with the dashed lines. We note that the 5-ns time limit corresponds to the crossover time from Rouse relaxation to entanglement controlled behavior recently found by NSE for long-chain PEB-2 melts at the same temperature.[7] The relaxation times for the first mode and for higher molecular weight also for the second mode deviate strongly from the Rouse behavior and increase much more rapidly—the upper solid line corresponds to a slope of $\tau \sim N^{3.8}$ with some uncertainty in the exponent.

Another aspect of the experimentally determined relaxation rates can be visualized if we plot W_p versus the mode number for different molecular weights. This is shown in Figure 7. For the sample with the lowest M_W the rates for all modes come out essentially identical. On the time scale of the experiment this chain undergoes Rouse dynamics though the diffusion coefficient is already reduced compared to the theoretical value for a Rouse chain $D_R = kT/N_p = Wl^2/3N = 14.3 \times 10^{-7}$ cm^2/s. Starting with the PE-3.6 sample, the rates for the lower modes are systematically reduced. While

Table 3. Results of the Mode Analysis and Comparison to the Macroscopic Diffusion (D_{NMR}) and Viscosity (η) Data by Pearson et al.[9]

sample	$W_p 10^{-11}$ $p=1$	$p=2$	$p=3$	$p>3$	$D_n \times 10^7$ (cm²/s)	$D_{NMR} \times 10^7$ (cm²/s)	η (P)	η_{cal} (P)
PE-2	4.6 ± 0.4	4.6 ± 0.4	4.6 ± 0.4	4.6 ± 1.0	8.6 ± 0.15	10.3	0.08	0.11 ± 0.012
PE-3.6	1.9 ± 0.2	5.0 ± 0.5	5.1 ± 0.5	5.1 ± 0.6	3.1 ± 0.16	3.6	0.35	0.38 ± 0.04
PE-4.8	1.0 ± 0.2	2.4 ± 0.4	4.1 ± 0.5	4.5 ± 1.0	1.9 ± 0.19	1.6	0.96	0.9 ± 0.18
PE-6.5	0.87 ± 0.16	0.87 ± 0.16	3.1 ± 0.4	5.6 ± 0.7	1.6 ± 0.18	0.57	1.84	1.64 ± 0.3

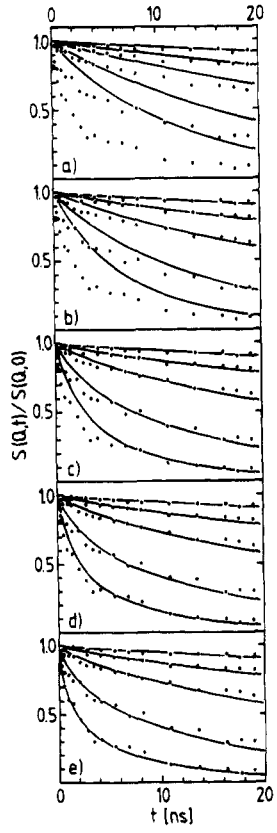

Figure 5. Result of the mode analysis for the sample PE-3.6. The figures present the resulting calculated spectra under inclusion of a successively increasing number of modes in comparison to the experimental points: (a) translational diffusion only, (b) translational diffusion and first mode, (c) translational diffusion and first two modes, (d) translational diffusion and first three modes, (e) translational diffusion and all modes.

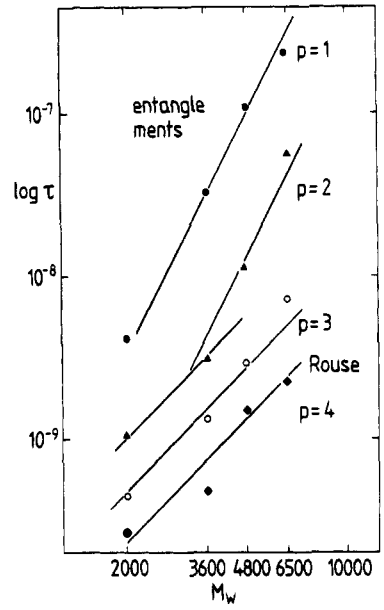

Figure 6. Mode relaxation times as obtained from the mode analysis as a function of molecular weight for the first four Rouse modes. The lower three solid lines indicate the Rouse prediction $\tau \propto M_W^2$. The upper two solid lines correspond to a power of 3.8.

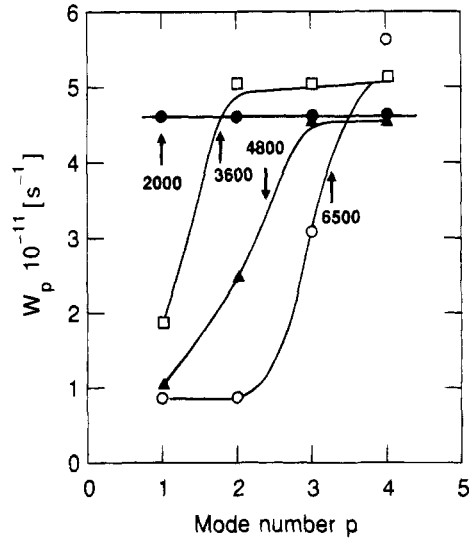

Figure 7. Relaxation rates W_p for the first four modes for chains of different molecular weight as a function of the mode number p. For each molecular weight the arrows indicate the condition $p = N/N_e$. The solid lines are guides to the eye.

for the PE-3.6 sample this relates only to the first mode, for large molecular weights higher modes are also affected.

As can be seen from a detailed comparison of the predicted curves to the experimental data, the agreement is not perfect (see Figures 1 and 5). In particular, at short times and for high molecular weights discrepancies occur. This suggests that the approach of an exponential correlation function for the normal modes may still be too rough. On the other hand, the mode analysis clearly shows an important and seemingly essential feature of the crossover to entanglement controlled dynamics. The long wavelength relaxation modes are strongly retarded, while the shorter wavelength modes are not affected.

This observation may be quantified in terms of the entanglement length d, which for long PEB-2 chains has been determined by NSE to be $d = 43.5$ Å[7] corresponding to $M_e = 2.0 \times 10^3$ or $N_e = M_0/m_0 = 138$ (m_0 = molecular weight/main-chain bond). The spatial extension of a mode p along the chain covers $n_p = N/p$ bonds. We now may ask how the slowing down of the first modes may be related to N_e. In Figure 7 $p_{cr} = N/N_e$ for different chains are indicated by arrows. Obviously, modes with $p \geq N/N_e$ are not modified, while modes with $p < N/N_e$ are strongly slowed down. This observation is equivalent to the earlier statement that above the crossover time to entanglement controlled behavior which has been determined on long-chain PEB-2 melts, even for much shorter chains the Rouse relaxation pattern ceases to be valid (Figure 6).

Summarizing the results from the mode analysis, the NSE experiments have led to some important insights into the process of entanglement formation. (i) The internal dynamics of short chains $N \leq N_e$ are well described by the Rouse model. (ii) If the chain length is increased beyond N_e internal modes, reflecting intrachain distances smaller than N_e persist, while relaxation modes corresponding to longer distances relax on a much longer time scale. Equivalently, we found that for short chains the mode relaxation at times longer than the crossover time to entanglement controlled behavior established for long-chain melts is strongly effected by topological constraints. (iii) The transition appears to be relatively sharp and is governed by M_e rather than by $M_c \approx 2.5M_e$, the critical molecular weight for the viscosity crossover.

At the end of this paragraph we compare the outcome of the mode analysis with recent diffusion and viscosity measurements on PEB-2 chains with different M_W by Pearson et al.,[9] which have been performed at $T = 175$ °C. In order to relate to our experiments carried out at $T = 236$ °C, we rely on extensive temperature- and M_W-dependent experiments on polyethylene again by Pearson et al.,[8] who explored the temperature shift factors for the monomeric friction coefficients over a large range of M_W and T (see Appendix I). As may be seen from Table 3 with the exception of the PE-6.5 sample, we found good agreement between the rescaled pulse field gradient NMR diffusion data of Pearson et al.[8] and our NSE results obtained at a much shorter length and time scale. The discrepancy at $M_W = 6.5 \times 10^3$ may be related to the shortness of our time scale ($t_{max} < 2 \times 10^{-8}$ s). At times much shorter than the relaxation time of the slowest internal mode ($\tau_1 = 2.3 \times 10^{-7}$ s) the center of mass motion may not yet have reached the asymptotic diffusion value (see the next paragraph).

In order to compare with the viscosity results, we resort to the general relation between viscosity and dynamic modulus $G(t)$ and internal relaxation times τ_i[20]

$$\eta = \int_0^\infty dt\, G(t) = \frac{\varrho N_A}{M}\frac{kT}{2}\sum \tau_i \qquad (6)$$

where ϱ is the polymer density and N_A Avogadro's number. Again assuming the above-mentioned $\varrho(M,T)$ relationship, we rescaled the viscosity results to 509 K. In Table 3 we compare them with a calculation on the basis of eq 6 using $\varrho(509\ K) = 0.733$ g/cm^3 and the rates of Table 3 converted to relaxation times following eq 5 (see also Figure 6). Figure 8 compares the calculated viscosities with the extrapolated data from Pearson et al. (see also Table 3). The agreement between macroscopic measurements and the calculation on the basis of a mode analysis of the dynamic structure factor is excellent, demonstrating the consistency of the results.

4. Generalized Rouse Model

In the preceding analysis, in a simple approximation we extracted the effect of topological constraints on "effective" mode relaxation rates. Now we want to become more ambitious and try to analyze the spectra in terms of an explicit model treating the influence of entanglement constraints on the chain motion.

4.1. The Hess Approach. Some years ago, on the basis of the excluded-volume interaction of chains, Hess[12] presented a generalized Rouse model in order to treat consistently the dynamics of entangled polymeric liquids. The theory treats a generalized Langevin

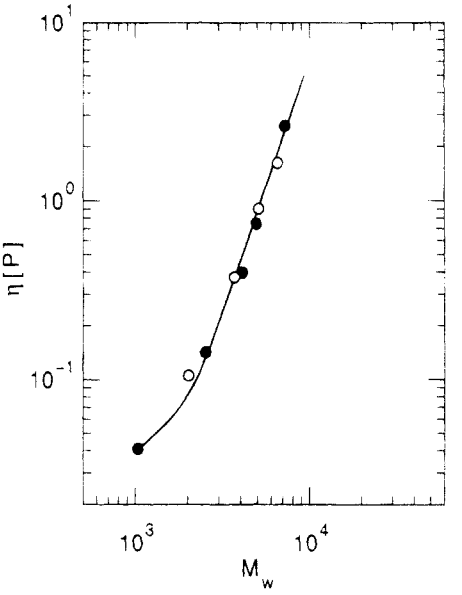

Figure 8. Rescaled and calculated viscosities for PEB-2 melts at 509 K as a function of molecular weight (●, experimental results;[8] ○, calculated viscosities on the basis of the mode analysis). The solid line serves as a guide to the eye.

equation where the entanglement friction function appears as a kernel of a memory function.

$$\frac{3kT}{l^2}(r_{n+1}(t) + r_{n-1}(t) - 2r_n(t)) + \zeta \dot{r}_n(t) + \sum_{n'}\int_0^t dt'\, \Delta\zeta_{nn'}(t-t')\, \dot{r}_{n'}(t')\, dt' = f_n(t) \qquad (7)$$

f_n are the random forces acting on segment n, and $\Delta\zeta_{nn'}(t)$ is the entanglement friction function. The entanglement friction function is calculated as the autocorrelation function of the excluded-volume forces. Though important approximations are involved, this approach goes beyond earlier phenomenological attempts, where $\Delta\zeta$ was derived from phenomenological arguments. In order to come to a treatable problem, a series of approximations were necessary.

(i) Via the excluded-volume forces the entanglement function $\Delta\zeta_{nn'}(t)$ depends on the dynamic four-point correlation function which cannot be calculated rigorously. $\Delta\zeta_{nn'}(t)$ was factorized with the argument that for a given segment not only its own collisions but also all other collisions along the chain are important. Therefore, the information on a specific collision decays on a fast time scale.

(ii) It was argued that the most pertinent contributions to $\Delta\zeta_{nn'}$ originate from the single segment propagator $G(Q,t)$. Consequently, the many-chain problem of eq 7 was reduced to a single-chain equation. In terms of $G(Q,t)$ the entanglement friction function reads

$$\Delta\zeta_{nn'} = \frac{4}{3}kT\frac{\psi}{N}\frac{v_0}{(2\pi)^3}\int d^3Q\, Q^2 G(Q,t)^2\, \delta_{nn'} \qquad (8)$$

Thereby, $\psi = N/N_c$ is the mean interaction energy of one chain in units of kT, N_c should correspond to N_e, the number of bonds between entanglements, and v_0 is the excluded-volume parameter. We remark that eq 8 contains the single segment propagator squared. Thus, not only the motion of the given chain but also that of the other chains are considered or constraint-release

mechanisms are automatically built in. This approach is similar to des Cloizeaux's recent double reptation idea.[21]

The segment propagator $G(Q,t)$ is approximated by

$$G(Q,t) = e^{-(D^{\parallel}+D^{\perp})q^2 t} e^{-W_{int}(t)\,q^2} \tag{9}$$

Thereby, $D^{\parallel}$ and $D^{\perp}$ are the center of mass diffusion coefficients parallel and perpendicular to the chain contour. Arguing that the center of mass diffusion should dominate the relaxation of entanglement friction, the second factor in eq 9 is neglected. With $\tau_e = [2(D^{\parallel} + D^{\perp})q_c^2]^{-1}$ where q_c^{-1} stands for the range of the chain interaction potential, eq 8 becomes

$$\Delta\zeta(t) = 4\frac{kT}{N_c} q_c^2 \int_0^2 dy\, y^4 \exp(-ty^2/\tau_e) \tag{10}$$

Thereby, τ_e is the characteristic time for the relaxation of the entanglement friction function. Taking $\Delta\zeta(t=0)$ and N_c as the two model parameters τ_e may be written as

$$\tau_e = \frac{N}{N_c}\frac{\zeta}{\Delta\zeta(0)}\begin{cases}\frac{2}{5}\left(1 - \frac{2}{3}\frac{N}{N_c}\right)^{-1} & N < N_c \\ \frac{6}{5} & N > N_c\end{cases} \tag{11}$$

Equations 9 and 10 define the entanglement friction function in the generalized Rouse equation (7) which now can be solved by Fourier transformation (Appendix II), yielding the frequency-dependent correlators $\langle x_p(\omega)\, x_{p'}(\omega')\rangle$. In order to calculate the dynamic structure factor following eq 2, the time-dependent correlators $\langle x_p(t)\, x_p(0)\rangle$ are needed. Beside the limiting cases of small and large ω which we discuss in the following, the backtransformation can only be performed numerically—we used the fast Fourier routine CO6FCF from the NAG library—resulting after insertion into eq 2 in a numerical expression for $S(Q,t)$.

The asymptotic short and long time behavior of the correlators can be accessed analytically. From eq B-12 we obtain by Fourier transformation

$$\langle x_p(t)\, x_p(0)\rangle = \frac{kT}{2N\tilde{\nu}_p}\left(\frac{\Delta\zeta(0)}{\zeta\tilde{\nu}_p} + e^{-\tilde{\nu}_p t}\left(1 - \frac{\Delta\zeta(0)}{\zeta\tilde{\nu}_p}\right)\right)$$

$$\text{with } \tilde{\nu}_p = \nu_p + \Delta\zeta(0)/\zeta \tag{12}$$

Other than in the Rouse model, where the correlations decay exponentially (eq 3), the effect of entanglement friction leads to an exponential decay of only part of $\langle x_p(t)\, x_p(0)\rangle$. There remains a time-independent plateau, the height of which depends via $\tilde{\nu}_p$ on the mode number and the relative strength of the entanglement friction $\Delta\zeta(0)$. This initial decay to mode-dependent plateaus coincides with the Ronca model in its limit for infinite chain length. If the modified Rouse rate $\tilde{\nu}_p$ becomes comparable with the entanglement friction rate $\Delta\zeta(0)/\zeta$, the modes do not decay—large-scale relaxations with low p are suppressed or strongly reduced.

From eq B-13 we obtain exponentially decaying correlators at long times

$$\langle x_p(t)\, x_p(0)\rangle = \frac{kT}{2N\zeta\nu_p}\exp\left(-\frac{\nu_p}{1 + 5/3\frac{\Delta\zeta(0)}{\zeta}\tau_e}t\right) \tag{13}$$

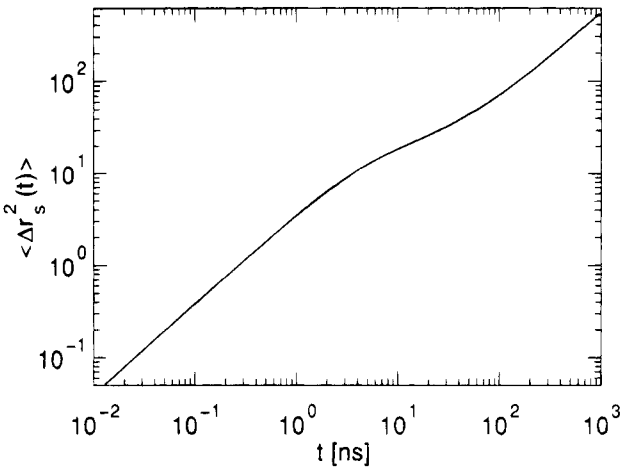

Figure 9. Mean-square center of mass displacement as a function of time as calculated on the basis of the parameters obtained from a fit of the spectra to the Hess model for a molecular weight of $M_W = 6500$.

Using $\tau_e = (6/5)(N/N_c)\zeta/\Delta\zeta(0)$ the relaxation times becomes

$$\tilde{\nu}_p = \nu_p(1 + 2N/N_c)^{-1} \tag{14}$$

which in the long chain limit agrees with the reptation prediction $\nu \sim 1/N^3$.

In order to assess the diffusion of the center of mass, we have to inspect the correlators $\langle x_0(\omega)\, x_0(\omega')\rangle$. At short times Fourier transformation of eq B-12 yields

$$\langle x_0(t)\, x_0(0)\rangle = \frac{kT}{N\zeta}\frac{\exp\left[-\left(\frac{1}{2}\frac{\Delta\zeta}{\zeta} + \left(\frac{\Delta\zeta}{\zeta}\left(\frac{\Delta\zeta}{\zeta}\frac{1}{4} + \frac{5}{7}\frac{1}{\tau_e}\right)\right)^{1/2}\right)t\right]}{\left[\frac{\Delta\zeta}{\zeta}\left(\frac{\Delta\zeta}{\zeta}\frac{1}{4} + \frac{5}{7}\frac{1}{\tau_e}\right)\right]^{1/2}} \tag{15}$$

resulting in a mean-square center of mass displacement

$$\langle (x_0(t) - x_0(0))^2\rangle = \frac{6kT}{N\zeta}\frac{1}{\left[\frac{\Delta\zeta}{\zeta}\left(\frac{1}{4}\frac{\Delta\zeta}{\zeta} + \frac{5}{7}\frac{1}{\tau_e}\right)\right]^{1/2}} \times$$

$$\left(1 - \exp\left[-\left(\frac{1}{2}\frac{\Delta\zeta}{\zeta} + \left[\frac{\Delta\zeta}{\zeta}\left(\frac{1}{4}\frac{\Delta\zeta}{\zeta} + \frac{5}{7}\frac{1}{\tau_e}\right)\right]^{1/2}\right)t\right]\right) \tag{16}$$

For short chains eq 16 reproduces the Rouse diffusion coefficient D_R (eq 3). For longer chains eq 15 predicts a highly nonlinear time dependence of the mean-square center of mass displacement, indicating an effective time-dependent diffusion coefficient. For long times with the help of eq B-13 we get

$$\langle [x_0(t) - x_0(0)]^2\rangle = 2\langle x_0(0)^2\rangle - 2\langle x_0(t)\, x_0(0)\rangle = \frac{2kT}{N\zeta(1 + 2N/N_c)}t \tag{17}$$

yielding $D = D_R(1 + 2N/N_c)^{-1}$. For large N the model reproduces the $1/N^2$ prediction of reptation.

The crossover time τ_D between both regimes is governed by the inverse decay rate of the correlator in eq 15 which by the aid of eq 11 reads for long chains $1/\tau_D = (1/2)(\Delta\zeta/\zeta)(1 + [1 + (50/21)(N_c/N)]^{1/2})$. In order to visualize a typical time-dependent diffusion coefficient, in Figure 9 we present the predicted mean-square center of mass displacement for the $M_W = 6500$ chain using

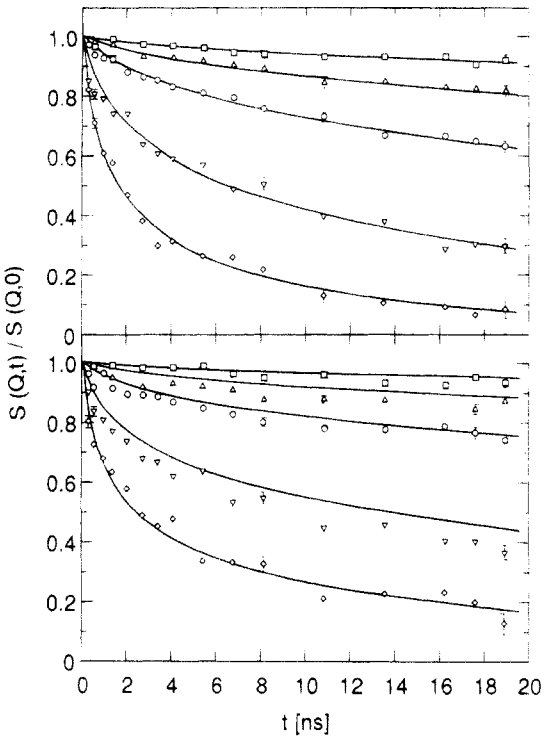

Figure 10. Experimental spectra for the samples PE-3.6 upper case, and PE-6.5 lower figure compared to the calculated spectra from the Hess model where the parameters have been obtained from a joint fit to all spectra (see text). The upper figure represents the case of best agreement, the lower figure the case of worst agreement.

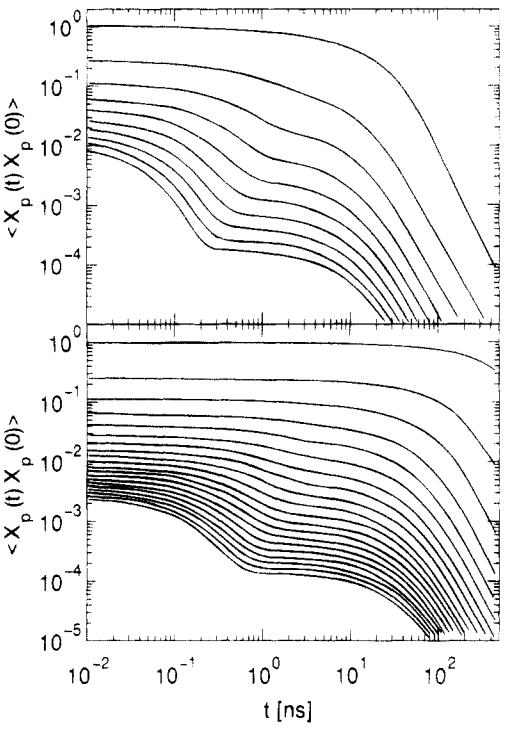

Figure 11. Time-dependent Rouse correlators for different Rouse modes. Upper figure for the molecular weight M_W = 2000; lower figure for the molecular weight M_W = 6500. The mode numbers increase from the top, commencing with p = 1. The time-dependent correlators were calculated with the parameters obtained from the joint fit (see text).

the evaluated model parameters. Within the experimental time range ($0.1 < t < 20$ ns) the crossover from short to long time behavior takes place. This clearly reveals the importance of the discussed time-dependent diffusion coefficient.

4.2. Comparison with Experiment. In addition to the Rouse model, the Hess theory contains two further parameters: the critical monomer number N_c and the relative strength of the entanglement friction $\Delta\zeta(0)/\zeta$. In order to fit the model to the data, we further have to consider that with decreasing molecular weight the monomeric friction coefficient of ζ decreases. Employing the molecular weight dependence as determined by Pearson et al.[8] (Appendix I) and using the asymptotic result $\zeta(M\to\infty)$ obtained in earlier experiments on long chains,[7] this parameter can be considered as known (the change of ζ with chain length amounts at maximum to 20% (PE-2)). The fit actually uses the Rouse rate Wl^4-$(M\to\infty)$ (eq 3) which was kept fixed at $Wl^4 = 6.8 \times 10^{13}$ Å^4 s^{-1}. The two remaining parameters N_c and $\Delta\zeta(0)/\zeta$ were determined in jointly fitting all experimental spectra to eq 2 inserting the correlators $\langle x_p(t)\, x_p(0)\rangle$ from the Fourier inversion of eq B-9. In this fitting procedure the time-dependent diffusion coefficient as discussed above has explicitly been taken into account. Figure 10 displays the calculated spectra in comparison with the experimental results for the PE-3.6 and PE-6.5 samples. As can be seen, with only two parameters both sets of spectra are well described. This holds also for the other two samples. For the model parameters the fit reveals $N_c = 150$ and $\Delta\zeta(0)/\zeta = 0.18$ ns^{-1}. N_c is very close to $N_e = 138$ as obtained from the NSE experiments on the PE-70 sample. According to Hess, the relative strength of the entanglement friction can be related to the more microscopic parameter q_c^{-1} describing the range of the true interchain interaction potential (eq 9). Combining eqs 9 and 3, we obtain $q_c^{-1} \simeq 7$ Å, a value close to the average interchain distance $s = m_0/l_0\varrho N_A \simeq$ 4.7 Å.

Thus, with only two parameters, the values of which are both close to expectation, the Hess model allows a complete description of all experimental spectra. In the complex crossover regime from Rouse motion to entanglement controlled behavior, this very good agreement can be considered as a significant success of this theory.

With the parameters obtained from the fit we have evaluated the time-dependent correlators $\langle x_p(t)\, x_p(0)\rangle$ of the Hess theory. Figure 11 presents results for the M_W = 2000 and M_W = 6500 cases. In both cases the correlators are plotted double-logarithmically as a function of time. The curves present the time-dependent relaxation of the different modes, commencing always with $p = 1$ at the top. In order to separate the different curves, they have been plotted including the $1/p^2$ prefactor. For the short chain the first modes exhibit significant relaxation within the experimental time frame ($0.1 < t < 20$ ns). In contrast, for the longer chains these modes relax only marginally and the main relaxation of the dynamic structure factor in the experimental time window is carried by the higher modes. The two-step relaxation exhibited by the higher p modes reflects the relaxation behavior displayed by eq 12. We observe a first decay to a plateau, the value of which depends on the mode number and for long times the final relaxation.

5. Summary and Conclusion

Using neutron spin-echo spectroscopy, we have investigated the space time evolution of large-scale relaxations in polymer melts, varying the molecular weight through the reptation transition. Exploiting the

Q-dependent onset of the contributions of different modes to the dynamic structure factor, we could access the first Rouse modes separately. We found that with increasing molecular weight the low numbered Rouse modes are significantly slowed down. Modes are affected if their spatial extension exceeds the entanglement mesh spanned by the entanglement distances obtained from measurements on long chains. Calculating the viscosity on the basis of the relaxation rates obtained from the mode analysis leads to excellent agreement with measurement viscosity data. In a second step we solved the equation of motions for the generalized Rouse model due to Hess and fitted the resulting dynamic structure factor to the experimental spectra. With only two parameters all experimental spectra taken from samples with four different molecular weights at five different Q values each could be described very well.

Acknowledgment. We thank the Laboratoire Léon Brillouin (Laboratoire Commune, CEA/CNRS), Saclay, France, for providing us with the necessary beam time at the MESS spin-echo spectrometer.

Appendix I

Recently, Pearson et al.[8] reported an extensive investigation of the temperature and molecular weight dependence of the monomeric friction coefficient ζ which has been found to follow with good accuracy a Vogel–Fulcher–Thamann relationship

$$\zeta = \zeta_\infty \exp\left\{\frac{B}{\Delta\alpha(T - T_0)}\right\} \tag{A-1}$$

with $\zeta_\infty = 3.7 \times 10^{11}$ dyn/cm and $B = 0.60$. Both the coefficient $\Delta\alpha$ and the Vogel–Fulcher temperature T_0 depend on molecular weight, reflecting the increase of free volume with decreasing chain length.

$$\Delta\alpha = \alpha_\infty(1 + \beta/M)$$

$$T_0 = T_0^\infty/(1 + \gamma/M) \tag{A-2}$$

with $\alpha^\infty = 5.1 \times 10^{-4}/C^0$, $\beta = 160$ g/mol, $T_0^\infty = 160$ K, and $\gamma = 80$ g/mol. Using eqs A1 and A2, the viscosity η may be rescaled according to

$$\eta(T_1) = \eta(T_0)\frac{\varrho(T_1)}{\varrho(T_0)}\frac{\zeta(T_1)}{\zeta(T_0)}\frac{T_1}{T_0} \tag{A-3}$$

where ϱ is the polymer density. For the diffusion coefficient we have

$$D(T_1) = D(T_0)\frac{T_1}{T_0}\frac{\zeta(T_0)}{\zeta(T_1)} \tag{A-4}$$

Using eqs A3 and A4, the quoted experimental data at 509 K in Table 3 were extrapolated from Pearson's data taken at 448 K.

Appendix II

Changing to continuous coordinates and using the approximations of eqs 8 and 9, the generalized Rouse equation (eq 7) becomes

$$\zeta\frac{\partial r_n}{\partial t} = \frac{3kT}{l^2}\frac{\partial^2 r_n}{\partial n^2} - \int_0^t \Delta\zeta(t - t')\frac{\partial r}{\partial t}\,dt' + f_n(t) \tag{B-1}$$

For the random forces we have

$$\langle f_n(t)\, f_{n'}(t')\rangle = 2kT\delta_{nn'}\{\zeta\delta(t-t') + \Delta\zeta(t-t')\} \tag{B-2}$$

According to eq 1, the spatial Fourier transformations (Rouse modes) are defined by

$$x_p(t) = \frac{1}{N}\sum_n r_n(t)\cos\left(\frac{p\pi n}{N}\right)$$

$$r_n(t) = x_0(t) + 2\sum_p x_p\cos\left(\frac{p\pi n}{N}\right) \tag{B-3}$$

With B-3 we obtain for the generalized Rouse modes x_p

$$\zeta\dot{x}_0 = -\int_0^t \Delta\zeta(t-t')\,\dot{x}_0(t')\,dt' + g_0$$

$$\zeta\dot{x}_p = -\frac{3kT}{l^2}\left(\frac{p\pi}{N}\right)^2 x_p - \int_0^t \Delta\zeta(t-t')\,\dot{x}_p(t')\,dt' + g_p \tag{B-4}$$

Fourier transformation of the random force correlation $\langle f_n(t)\, f_{n'}(t')\rangle$ yields

$$\langle g_p(t)\, g_p(t')\rangle =$$

$$\frac{2kT}{N}\{\zeta_0\delta(t-t') + \Delta\zeta(t-t')\}\begin{cases}1/2 & p > 0\\ 1 & p = 0\end{cases} \tag{B-5}$$

Defining the temporal Fourier transformation by

$$\tilde{x}(\omega) = \frac{1}{(2\pi)^{1/2}}\int_{-\infty}^{+\infty} e^{-i\omega t}x(t)\,dt \tag{B-6}$$

Equation B-4 can be readily Fourier transformed, resulting in

$$\tilde{x}_p(\omega) = \frac{\tilde{g}_p(\omega)}{\left(\frac{\pi p}{N}\right)^2\frac{3kT}{l^2} + i\omega(\zeta_0 + (2\pi)^{1/2}\Delta\tilde{\zeta}(\omega))} \tag{B-7}$$

For the random force correlators we get

$$\langle \tilde{g}_p(\omega)\,\tilde{g}_p(\omega')\rangle =$$

$$(2)\frac{kT}{N}\delta_{pp'}\{\zeta + (2\pi)^{1/2}\Delta\tilde{\zeta}(\omega)\}\delta(\omega+\omega') \tag{B-8}$$

The correlation functions $\langle x_p(\omega)\, x_p(\omega')\rangle$ become

$$\langle x_p(\omega)\, x_p(\omega')\rangle =$$

$$\frac{kT}{N\zeta}\frac{\left(1 + (2\pi)^{1/2}\dfrac{\Delta\tilde{\zeta}(\omega)}{\zeta}\right)\delta(\omega+\omega')}{\text{denominator}} \qquad p > 0$$

$$\text{denominator} = \nu_p^{\,2} - 2\omega\nu_p(2\pi)^{1/2}\mathrm{Im}\Delta\tilde{\zeta}(\omega)/\zeta + \omega^2(1 + 2(2\pi)^{1/2}\mathrm{Re}\Delta\tilde{\zeta}(\omega)/\zeta) + 2\pi|\Delta\zeta(\omega)/\zeta|^2$$

$$\langle x_0(\omega)\, x_0(\omega')\rangle =$$

$$\frac{2kT}{N\zeta\omega^2}\frac{\delta(\omega+\omega')}{1 + (2\pi)^{1/2}\Delta\zeta(-\omega)/\zeta} \qquad p = 0 \tag{B-9}$$

Finally we have to calculate the Fourier transformed friction function (eq 9)

$$\Delta\tilde{\xi}(\omega) = \frac{5}{(2\pi)^{1/2}}\Delta\xi(0)\tau_e\left\{1 - \frac{1}{3}\tau_e\omega - 3(-1)^{3/4}(\tau_e\omega)^{3/2} \arctan\left(\frac{(-1)^{3/4}}{(\omega\tau_e)^{1/2}}\right)\right\} \quad \text{(B-10)}$$

For small and larger $\omega\tau_e$, $\Delta\tilde{\xi}(\omega)$ can be expanded into a Taylor series

(i) $\omega\tau_e \gg 1$

$$\Delta\tilde{\xi}(\omega) \simeq \frac{5\Delta\xi(0)}{(2\pi)^{1/2}}\tau_e\left\{-\frac{i}{5\omega\tau_e} + \frac{1}{7}\frac{1}{(\omega\tau_e)^2} + \frac{i}{9}\frac{1}{(\omega\tau_e)^3}\cdots\right\}$$

(ii) $\omega\tau_e \ll 1$

$$\Delta\tilde{\xi}(\omega) \simeq \frac{5\Delta\xi(0)}{(2\pi)^{1/2}}\tau_e\left\{\frac{1}{3} - i\omega\tau_e + \frac{(-1)^{3/4}\pi}{2}(\omega\tau_e)^{3/2} + (\omega\tau_e)^2 - \ldots\right\} \quad \text{(B-11)}$$

With this expansion approximate expressions for the correlation functions may be obtained

(i) high $(\omega\tau_e)$

$$\langle x_p(\omega)\, x_p(\omega')\rangle \simeq \frac{kT}{N\zeta}\frac{\left(1 - i\frac{\Delta\zeta(0)}{\zeta}\right)\delta(\omega+\omega')}{\left(\nu_p + \frac{\Delta\zeta(0)}{\zeta}\right)^2 + \omega^2} \qquad p > 0$$

$$\langle x_0(\omega)\, x_0(\omega')\rangle = \frac{2kT}{N\zeta}\frac{\delta(\omega+\omega')}{\omega^2 + \frac{5}{7}\frac{\Delta\zeta}{\zeta\tau_e} + i\omega\frac{\Delta\zeta}{\zeta}} \qquad p = 0 \quad \text{(B-12)}$$

(ii) low $(\omega\tau_e)$

$$\langle x_p(\omega)\, x_p(\omega')\rangle = \frac{kT}{N\zeta}\frac{\left(1 + \frac{1}{3}\frac{5\Delta\zeta(0)}{\zeta}\tau_e\right)\delta(\omega+\omega')}{\omega^2\left(1 + \frac{5}{3}\frac{\Delta\zeta(0)}{\zeta}\tau_e\right)^2 + \nu_p{}^2}$$

$$\langle x_0(\omega)\, x_0(\omega')\rangle = \frac{2kT}{N\zeta\omega^2}\frac{\delta(\omega+\omega')}{\left(1 + \frac{5}{3}\frac{\Delta\zeta(0)}{\zeta}\tau_e\right)} \quad \text{(B-13)}$$

All these approximate expressions can be Fourier transformed analytically into the time domain, revealing the asymptotic expressions for the correlators $\langle x_p(t)\, x_p(0)\rangle$.

References and Notes

(1) Ferry, J. D. *Viscoelastic Properties of Polymers*; Wiley: New York, 1980.
(2) Doi, M.; Edwards, S. F. *The Theory of Polymer Dynamics*; Clarendon: Oxford, U.K., 1986.
(3) de Gennes, P.-G. *J. Chem. Phys.* **1971**, *55*, 572.
(4) Doi, M.; Edwards, S. F. *J. Chem. Soc., Faraday Trans. 2* **1978**, *74*, 1789; **1978**, *74*, 1802; **1978**, *74*, 38.
(5) Russel, T. P.; Deline, V. R.; Dozier, W. D.; Felcher, G. P.; Agrawal, G.; Wool, R. P.; Mays, J. W. *Nature* **1993**, *305*, 235.
(6) Richter, D.; Farago, B.; Fetters, L. J.; Huang, J. S.; Ewen, B.; Lartigue, C. *Phys. Rev. Lett.* **1990**, *64*, 1389.
(7) Richter, D.; Butera, R.; Fetters, L. J.; Huang, J. S.; Farago, B.; Ewen, B. *Macromolecules* **1992**, *25*, 6156.
(8) Pearson, D. S.; Ver Strate, G.; von Meerwall, E.; Schilling, F. C. *Macromolecules* **1987**, *20*, 1133.
(9) Pearson, D. S.; Fetters, L. J.; Graessley, W. W.; Ver Strate, G.; von Meerwall, E. *Macrmolecules* **1994**, *27*, 711.
(10) Richter, D.; Farago, B.; Butera, R.; Fetters, L. J.; Huang, J. S.; Ewen, B. *Macromolecules* **1993**, *26*, 795.
(11) Rouse, P. E. *J. Chem. Phys.* **1953**, *21*, 1273.
(12) Hess, W. *Macromolecules* **1988**, *21*, 2620.
(13) A short account of this work has been given in: Richter, D.; Willner, L.; Zirkel, A.; Farago, B.; Fetters, L. J.; Huang, J. S. *Phys. Rev. Lett.* **1993**, *71*, 4158.
(14) Chu, B.; Wang, Zh.; Yu, J. *Macromolecules* **1991**, *24*, 6832.
(15) Gehlsen, M. D.; Bates, F. S. *Macromolecules* **1983**, *26*, 4122.
(16) Mezei, F. In *Lecture Notes in Physics*; Mezei, F., Ed.; Springer-Verlag: Berlin, Heidelberg, New York, 1980; Vol. 128.
(17) Ronca, G. J. *J. Chem. Phys.* **1983**, *79*, 79.
(18) de Gennes, P.-G. *Physics (Long Island City N.Y.)* **1967**, *3*, 37.
(19) Boothroyd, A. T.; Rennie, A. R.; Boothroyd, C. B. *Europhys. Lett.* **1991**, *15*, 715.
(20) Graessley, W. W. *Adv. Polym. Sci.* **1974**, *16*, 1.
(21) des Cloizeaux, J. *Macromolecules* **1990**, *23*, 3992.